ITN-5VC

Integrated Telematics for Next Generation 5G Vehicular Communications

ITN-5VC D1.2

Report on guidelines for OTA characterization of phased array MIMO antennas for 5G V2X applications

Version v1.0 Date: 2023/03/24

Document properties:

Grant Number:	955629
Document Number:	D1.2
Document Title:	Report on guidelines for OTA characterization of phased array MIMO antennas for 5G V2X applications
Partners involved:	University of Twente, Bluetest
Authors:	Alejandro Antón Ruiz and Andrés Alayón Glazunov (Editor)
Contractual Date of Delivery:	2023/03/31
Dissemination level:	CO[1]
Version:	1.0
File Name:	ITN-5VC D1.2_v1.0

[1] CO = Confidential, only members of the consortium (including the Commission Services)
PU = Public

Table of Contents

Executive summary

This deliverable presents a report on guidelines and simulations for OTA characterization of phased array MIMO antennas for V2X applications, as well as results from actual measurements at mmWave frequencies. The objectives of this report are to provide insights on the characterization of a quiet zone within an OTA testing system using several FoM, along with the impact of excitation and weighting errors on MIMO performance, in the context of a compact OTA setup. Additionally, the methodology to make measurements with a phased array at mmWave frequencies in a Bluetest reverberation chamber is carefully explained, including several practical considerations that must be accounted for, along with some of the obtained results and statistical analysis. Part of the results presented in this report have been summarized in paper [A], which has been already accepted and will be presented during EuCAP2023. In addition, the measurement results here presented are intended to be used to produce a contribution for ISAP2023 conference, which is still under development.

[A] A. Antón Ruiz, A. A. Glazunov, “Impact of Excitation and Weighting Errors on Performance of Compact OTA Testing Systems” EuCAP2023.

List of figures

List of tables

List of acronyms and abbreviations

ADAS	Advanced Driver Assistance Systems
AE	Antenna Elements
CATR	Compact Antenna Test Range
CDF	Cumulative Distribution Function
CW	Continuous Wave
DUT	Device Under Test
FoM	Figures of Merit
IA	Interferer Array
IES	Inter-Element Spacing
JCAS	Joint Communication And Sensing
LOS	Line-Of-Sight
MA	Main Array
MF	Matched Filter
MIMO	Multiple-Input Multiple-Output
mmWave	millimeter wave
MPAC	Multiprobe Anechoic Chamber
OTA	Over-the-air
PWG	Plane Wave Generator
RIMP	Rich Isotropic Multipath
SINR	Signal to Interference plus Noise Ratio
SNR	Signal to Noise Ratio
TRP	Total Radiated Power
TZ	Test Zone
ULA	Uniform Linear Array
VNA	Vector Network Analyzer
WP1	Work Package 1
ZF	Zero Forcing

1 Introduction

Among the objectives of Work Package 1 (WP1), there is the development of cost-effective over-the-air (OTA) characterization methods and figures of merit (FoM) to reflect system performance of phased array Multiple-Input Multiple-Output (MIMO) antennas at millimeter wave (mmWave). In addition, guidelines on the deployment and OTA characterization of mmWave MIMO antennas mounted on cars should be devised.

WP1 is mainly contributed by ESR 1, ESR 2, ESR 3, ESR 4 and ESR 7. The Deliverable 1.2 presented here shows the characterization of an OTA test system at mmWave, as well as the measurement procedure and results of a mmWave phased array at 5G FR2 frequencies, obtained during the secondment of ESR 2 at Bluetest.Characterization of a compact mmWave OTA testing solution.

1.1 Automotive OTA testing

OTA testing has become the standard for evaluating the performance of wireless communication devices due to its realistic characterization of the actual performance of the device including the antennas. In addition, miniaturization of antenna systems, especially for mmWave, where the access to the antenna ports is not possible has made OTA testing indispensable. However, OTA faces a series of challenges in different applications, such as the automotive industry to which the ITN-5VC project is dedicated to.

The automotive industry can benefit substantially from advances in OTA testing solutions for current and future systems. This is mainly because current and future trends are focused on the integration of an increasing number of sensors, e.g., lidars, radars, cameras, along with GPS and mobile communications. In particular, OTA testing can be used to assess the performance of GPS, radar and mobile communications.

Moreover, all new automotive radar modules are using an operating frequency of 76 to 81 GHz, since the 24 GHz band has been phased out. Vehicle-to-Everything (V2X) communications today operate just in the sub-6 GHz bands. However, it is expected that V2X goes up in frequency in the future to mmWave frequencies, such as the ones belonging to the FR2 frequency bands, a subset of which can be observed in Figure 1. This would enable some use cases such as the exchange of raw sensor data between vehicles to improve the perception of autonomous vehicles or vehicles equipped with Advanced Driver Assistance Systems (ADAS) due to the larger available bandwidths at mmWave frequencies. In addition, there is a current trend towards the integration of communication and sensing, being Joint Communication And Sensing (JCAS) one of the ways to designate such systems. In the case of automobiles, such systems, due to resolution requirements, would take place at mmWave frequencies.

In addition, MIMO systems are already a standard both in mobile communications and radar, and higher order MIMO systems will be used in upcoming mmWave communication systems.

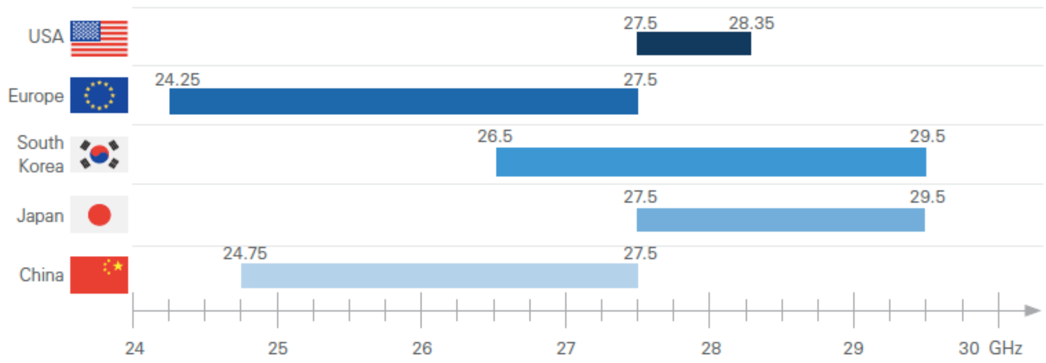

Figure 1. 28 GHz Spectrum Availability, Courtesy of CEPT

Currently, OTA testing of MIMO mmWave communication devices is already in the market, although only for relatively small form factors, such as mobile phones or even base stations. Additionally, automotive radar OTA testing solutions exist, both with the radar standing alone as well as with it mounted on the vehicle. Nevertheless, there is a lack of solutions for mmWave MIMO OTA testing solutions for large scale form factors, in particular, automobiles, both for radar and communications considered as detached systems, and especially for JCAS systems, due to the nonexistence of standardized, commercial automotive JCAS systems.

1.2 Main OTA testing solutions

1.2.1 Anechoic chambers

Anechoic chambers are used to emulate free space propagation conditions using absorbers to avoid any reflections coming from the ground, walls, or ceiling, as well as the different components of the chamber such as an antenna positioner.

One of their applications is to generate complex spatio-temporal channels to approximate realistic wireless channel conditions, through the use of multiple probes around the test zone (TZ), weighted to generate almost plane waves in that zone, as well as multi-channel wireless channel emulators. This is known as Multiprobe Anechoic Chamber (MPAC). These solutions are especially well suited to emulate MIMO channels, however, there is an increase in the number of probe antennas required to generate the desired channel realization for a given physical size of a TZ increase with the frequency, due to the increase in electrical size of the TZ, or for a fixed frequency, if the TZ physical size is larger. The channel emulators must also support the increased number of antennas. This makes MPAC not economically or even technically (e.g. limitations of channel emulators channels) feasible for physically large TZs combined with mmWave frequencies.

Another application is to measure the (far-field) radiation pattern of the Device Under Test (DUT), although this is not exclusively done in full anechoic chambers, being also possible to use semi-anechoic chambers. In this application, the DUT must be in the far-field of the measurement antenna (e.g., a horn antenna), but that is not always possible or convenient size and cost-wise. Therefore, there are alternatives to generate far-field conditions (i.e., impinging plane wave). One of them is the use of a feeder and a reflector, in what is known as a Compact Antenna Test Range (CATR) system. Another relevant solution is the use of Plane Wave Generators (PWGs), which use an antenna array to synthesize a plane wave, while being within the near field of the array. PWGs will need more sources as the electrical size of the TZ in which a plane wave like electric field distribution increases. A system that allows to test the communication performance of wireless devices is the so called Random Line-Of-sight (Random-LOS) setup that generates a plane wave in the test zone where a DUT or a vehicle shall be placed and rotated during measurements.

In these chambers, the random Line-Of-Sight (LOS) test environment can be implemented. In the case of mobile phones, then the randomness should be 3D to be realistic, although in vehicles, it can be argued that a 2D randomness (e.g., coming from the rotation of the vehicle in a turntable) can be enough to assess the performance in most common situations.

1.2.2 Reverberation chambers

Reverberation chambers are closed cavities made of reflective materials, which will resonate when RF signals are feeded into them. They emulate a Rich Isotropic Multipath (RIMP) electric field distribution, achieving a close to Rayleigh distribution of the magnitude of the electric field, as well as an exponential power distribution. This is achieved thanks to the use of mode stirrers, which can be metallic plates or the turntable itself, which, by moving, will change the boundary conditions of the chamber and, consequently, the interference of the multiple signal bounces in the chamber will result in a different magnitude of the electric field at the DUT. It must be noted that the chamber is excited by one or more antennas behind a metallic plate, so that the LOS component to the DUT is blocked.

These chambers are especially well suited for active measurements such as Total Radiated Power (TRP) or total isotropic sensitivity, as well as passive ones such as MIMO diversity and capacity. However, they are not generally suitable for measuring radiation patterns or generating channels different to RIMP.

1.2.3 Drive tests

This solution consists in the measurement of the realized performance of the DUT in the real world. In the case of automobiles, it consists in driving through a set route and gathering the corresponding performance data. This method is the most straightforward in terms of the required setup, since the infrastructure for testing already exists, and it also provides an example of the real-world performance of the DUT.

However, this solution has multiple inconveniences which make it unfeasible in practical terms. First, the repeatability of the measurement is extremely limited, since it will not be possible to control the environment to the extent that the exact same conditions are met. On the other hand, the test will require a lot of resources both in time and money, since many parallel measurements might need to be conducted due to the lack of repeatability, and the measurements must actively be supervised by humans.

1.3. Automotive mmWave MIMO OTA testing challenges

As it has been exposed in the previous sections, OTA testing at mmWave and with large TZs to fit large DUTs such as automobiles is challenging. On the one hand, drive tests are not a good testing solution in general, but, in case a new JCAS system was tested and was not supported by the infrastructure (i.e. the cellular network), then it would not be feasible.

As for the reverberation chambers, they might be suitable in terms of size to fit a vehicle inside them and be able to do active and passive measurements. However, it will not be possible to emulate controlled LOS scenarios (pure LOS, like Random-LOS, or Rician channels), which are the most probable situations in which an automobile would operate, especially at mmWave. Therefore, a reverberation chamber by itself might not be enough to fully evaluate the performance of a MIMO communications system in a vehicle at mmWave.

As for the anechoic chambers, the MPAC approach is directly unfeasible in terms of hardware costs and complexity if the whole vehicle is within the zone in which the field distribution emulates the desired channel. As previously mentioned, Random-LOS is a good scenario to emulate for evaluating automotive RF performance. For that, it is needed to have a TZ where the car fits that has a field distribution as similar as possible to the one that would happen in the far-field.

One of the main challenges for a system in which it is desired to have far-field like field distribution (i.e., plane wave) is that the Fraunhofer distance is proportional to the square of the TZ largest dimension, and it is inversely proportional to the wavelength. Therefore, the combination of a large physical size of a TZ that could fit a car with the small wavelength of mmWave results in a Fraunhofer distance in the order of the kms. That is, for obvious reasons, unfeasible.

One solution to this problem can be to measure in the near-field and then perform a near to far-field transformation, although it might not always be possible due to the use of active antennas as DUTs, since the phase information is required and cannot be directly obtained when measuring active antennas, as it would with passive ones. Then, we also have the PWG and CATR, which try to achieve that far-field like distribution in the near-field, but it needs to be evaluated if they can do it at a reasonable cost, while also fulfilling requirements such as MIMO measurements.

When designing CATR or PWGs, it needs to be considered that the simulations will differ from the actual manufactured product. This can come from excitation errors of the PWG sources, manufacturing tolerances of the CATR reflector or the PWG sources position, different antenna efficiencies of the PWG sources, misalignments between the feed and the reflector of a CATR due to mechanical properties of the materials …

Consequently, it needs to be evaluated which would be the impact of the different sources of errors and how much of these errors can be tolerated by the design and compare them to the margins of error of, e.g., the manufacturing process. All this needs to be done with the objective that the manufactured, real system satisfies the requirements and meets the performance needed to be considered a valid OTA testing solution.

2. Compact random-LOS OTA testing system at mmWave

As a first step within this project to achieve a MIMO OTA testing solution for vehicles at mmWave, a study on the TZ characterization using a Uniform Linear Array (ULA) was performed, followed by an analysis of the impact of excitation and weighting errors on the performance of the system. This was conducted in a scenario which could be achieved with an anechoic chamber and at 28 GHz of frequency, which is the center frequency of the n257 5G band, used in South Korea as one of the 5G FR2 bands (see Figure 1). Even though the test zone is far less large than what would be needed for a vehicle and it is limited to just 2D, it can be considered as a first step and to illustrate the methodology to design a system which can fulfil a series of requirements, among which the compactness of the system will be relevant, which has been pursued in this study, although proper optimization should still be carried out. In the future, throughout the duration of the project, this will be used as a base to design a more sophisticated system that fits the project's needs, including JCAS testing, which is not considered here. Additionally, this study investigates two different sources of error, namely the chamber array excitation error and its impact on the test zone quality and the weighting of DUT error and its impact on the performance of Zero Forcing (ZF) and Matched Filter (MF) algorithms. The objective of this part of the study, aside from the assessment of the errors and their effects on this particular setup, is to develop a method to evaluate, through simulations, the impact of different sources on error, to pave the way to a future holistic design of an OTA testing system for automobiles at mmWave that takes into account not only the idealized simulations, but also incorporates real life effects of manufacturing tolerances and several imperfections which, if not accounted for in the design process, could lead to a failure of the manufactured system. The study presented here is based on the already accepted EuCAP conference paper that will be presented the 31st of March [A].

2.1. Setup

The proposed OTA testing system, as seen in Figure 2, which is not to scale, consists in a ULA of $N_C = 100$ Antenna Elements (AEs), which will act as the chamber array, responsible for generating the desired electric field distribution at the circular, 2D test zone of radius R, the center of which is at a distance D from the ULA. Free space propagation is assumed, similar to what would happen in an anechoic chamber. The AEs of the ULA are considered vertically polarized (z-axis), ideal isotropic sources, operating at 28 GHz. A linear taper from 0 dB to -6 dB is applied to 25 elements on each side of the array to reduce field fluctuations in the TZ, as will be explained later.

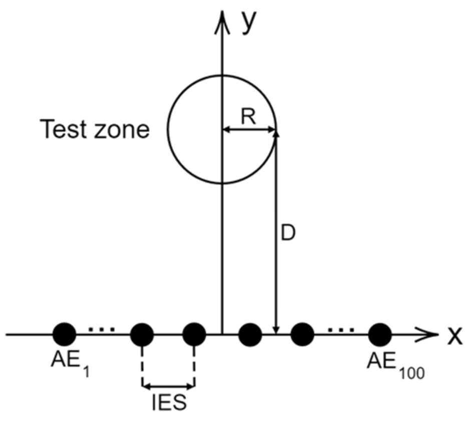

Figure 2. OTA setup

The electric field at a given point *P* will be computed using the superposition principle, and since only the E_z component of the electric field is not null, then at point *P*, we have that

$$E_z = \sum_{i=1}^{N_C} t_{c_i} E_0 \frac{e^{-jkr_i}}{4\pi r_i} = \sum_{i=1}^{N_C} t_{c_i} \frac{e^{-jkr_i}}{4\pi r_i}, \tag{1}$$

where E_0 is considered 1 for the sake of simplicity, r_i is the distance between the point *P* and the i-th AE, and $t_{c_i} = 10^{t_{c_{i_{dB}}}/20}$ is the tapering coefficient of the i-th AE in linear units, while $t_{c_{i_{dB}}}$ is the tapering coefficient in logarithmic scale. The Inter-Element Spacing (IES) is a variable, with a range of 0.5λ to 1.5λ, with a 0.05λ step. Consequently, the chamber array has a range of lengths defined by $L = (N_C - 1)IES$. Then, as for the radius of the test zone R, we define it as $R = (N_C - 1)IES/4$, where IES is equal to half a wavelength (0.5λ). Therefore, $R = 99\lambda/8 = 13.26$ cm, which corresponds to a quarter of the length of the shortest chamber array considered here.

2.2. TZ characterization and FoM to assess test zone quality

When designing a Random-LOS OTA testing system, one of the main points to accomplish is to get a far-field like field distribution in the desired TZ, which needs to be at least as large as the DUT. In this case, the field distribution will be that of a plane wave, so that the effect of the DUT antennas can be extracted from the measurement system without any distortion of the placement of the DUT within the TZ. For example, if an OTA testing system is being designed for automobiles in general, then it should be able to measure different vehicles with different antenna placements in the same way (at least within some tolerance or uncertainty margins).

Therefore, it must be ensured that the field distribution in the TZ is that of a plane wave, and, for that, it is necessary to stablish a series of FoM that will be used throughout the design process to achieve a certain degree of resemblance to the plane wave field distribution.

First of all, the TZ is sampled using a mesh with $\lambda/8$ spacing in the x-axis as well as the y-axis. Thus, the density of samples remains constant through all the circular TZ.

The first FoM we define is R_{mag}, which is the dynamic range of the magnitude of the electric field at a sampled point of the TZ and is defined as follows

$$R_{mag} = \max\left(20\log10\left(|\boldsymbol{E}_z|\right)\right) - \min\left(20\log10\left(|\boldsymbol{E}_z|\right)\right), \tag{2}$$

where $|\boldsymbol{E}_z|$ is the magnitude of the electric field through all the TZ. In an ideal scenario, the magnitude of the electric field should be practically constant throughout the TZ, although it is not possible that it has the exact same value for a system as the one considered. Therefore, the ideal value of R_{mag} would be 0 dB. The commonly accepted value of this FoM is $R_{mag} \leq 1$ dB [1].

Then, we define σ_{mag}, which is the standard deviation of the magnitude of the electric field in dB, as follows

$$\sigma_{mag} = \sqrt{\frac{\sum_{s=1}^{N_s}(X_s - \bar{x})^2}{N-1}}, \tag{3}$$

where N corresponds to the number of TZ samples, $\bar{x}$ is the mean electric field magnitude of all the TZ samples, and X_s is the electric field magnitude in log scale of the s-th sample. Following the same reasoning as with R_{mag}, we have that the ideal but unachievable value of σ_{mag} would be 0 dB. However, the required value of σ_{mag} from the 3GPP standards is $\sigma_{mag} \leq 0.25$ dB [2].

Finally, we define R_{phs}, which is the maximum phase range of all the parallel stripes of the TZ (each stripe has a constant y value, so they are parallel to the chamber array). The following equations define this FoM

$$R_{phs_{rows_n}} = \max(\angle \mathbf{E}_{z_n}) - \min(\angle \mathbf{E}_{z_n}), \tag{4}$$

$$R_{phs} = \max(\mathbf{R}_{phs_{rows}}), \tag{5}$$

where $\mathbf{R}_{phs_{rows}}$ is the phase range of every TZ parallel stripe, $R_{phs_{rows_n}}$ is the phase range of the n-th stripe and $\mathbf{E}_{z_n}$ is the electric field of each of the samples contained by the n-th stripe. Note that $\angle$ denotes angle (phase in this case). This FoM has a target value of 0º, i.e., that the phase is constant along every TZ stripe parallel to the chamber array. The acceptable limit of this FoM is usually $R_{phs} \leq 10º$ [3].

2.3. Design of a compact Random-LOS OTA testing system

Having established the FoM and their respective acceptable values, now the focus goes into devising a setup which is as compact as possible, since that is one of the requirements that an automotive OTA testing system would have. Therefore, there are two parameters that play a role on the compactness of the setup. The first of them is the length of the chamber ULA, which is defined by L and depends on the IES, since the number of sources has been fixed to 100 to limit the cost that such a system would have to a reasonable level. The other would be the distance D between the chamber array and the center of the TZ. This defines in a rough sense the size of the chamber. The objective is to have a set of L and D which are the smallest possible, while still fulfilling the FoM requirements.

Hence, we take a parameter sweep approach of L and D. The values of L come from considering an IES of 0.5λ up to 1.5λ, with a 0.05λ step. Then D ranges from 40λ to 2450λ, corresponding the latter value to approximately half of the Fraunhofer distance of the shortest (0.5λ IES) considered chamber array. Then the FoM values are computed for each combination of L and D and then it is observed whether the three of them are within the acceptable limits or not.

During this study, it was observed that if a linear tapering was applied to the ULA, then more compact setups would fulfill the FoM. This was inspired by [4], and some variations of the linear tapering were considered, deciding to use 0 dB to -6 dB of linear tapering applied to 25 elements on each side of the array. Nevertheless, no optimization or parameter sweep was done when deciding which tapering was the best to comply with the FoM with the most compact setups.

So, there is room for improvement if an optimization or, at least, parameter sweep is done in the future.

Even though the objective is to have the FoM at a level within the accepted values of them, since these are simulations free of errors, then we should keep some headroom for such errors. Therefore, three tiers of accomplishment of the FoM are defined. The first of them is the less strict one, with the literature accepted values of $R_{mag} \leq 1\ dB$, $\sigma_{mag} \leq 0.25\ dB$, and $R_{phs} \leq 10º$. Then, the second tier has $R_{mag} \leq 0.9\ dB$, $\sigma_{mag} \leq 0.225\ dB$, and $R_{phs} \leq 9º$. And finally, the third tier has $R_{mag} \leq 0.8\ dB$, $\sigma_{mag} \leq 0.2\ dB$, and $R_{phs} \leq 8º$. It can be argued if the decrease on the acceptable levels should be done in the way that was done in this study, but it was not possible to find any literature that could indicate how the proportionality between the reduction of each FoM limit should be established. Hence, it was opted to use a very simplistic approach.

In the plots from Figures 3, 4 and 5, whenever the color is light grey, then the three FoM limits are fulfilled. Conversely, when the color is dark grey, then the FoM limits are not achieved by at least one of the three FoM.

From the figures, it can be observed that there are multiple combinations of L and D that provide a relatively compact setup, since, for example, some of the points have a D of around a 5% of the Fraunhofer distance of the shortest considered chamber array, and less than a 5% of the Fraunhofer distance corresponding to the L and D combination at that point. Aside from that, it is noticeable that there is not linearity in the combinations and some of the results are counterintuitive, since, for example, increasing D does not always mean a better result, i.e., a point with L_1 and D_1 complies with the FoM, and then, a second point with L_1 and $D_2 > D_1$ does not comply with the FoM. However, there are somewhat curves of complying combinations of L and D. Finally, if one goes to the most compact setups possible (see the yellow points at Figures 4 and 5), from both chamber array and chamber dimensions, then it can be observed that there is a trade-off between L and D, so larger arrays allow smaller chamber sizes and the other way around.

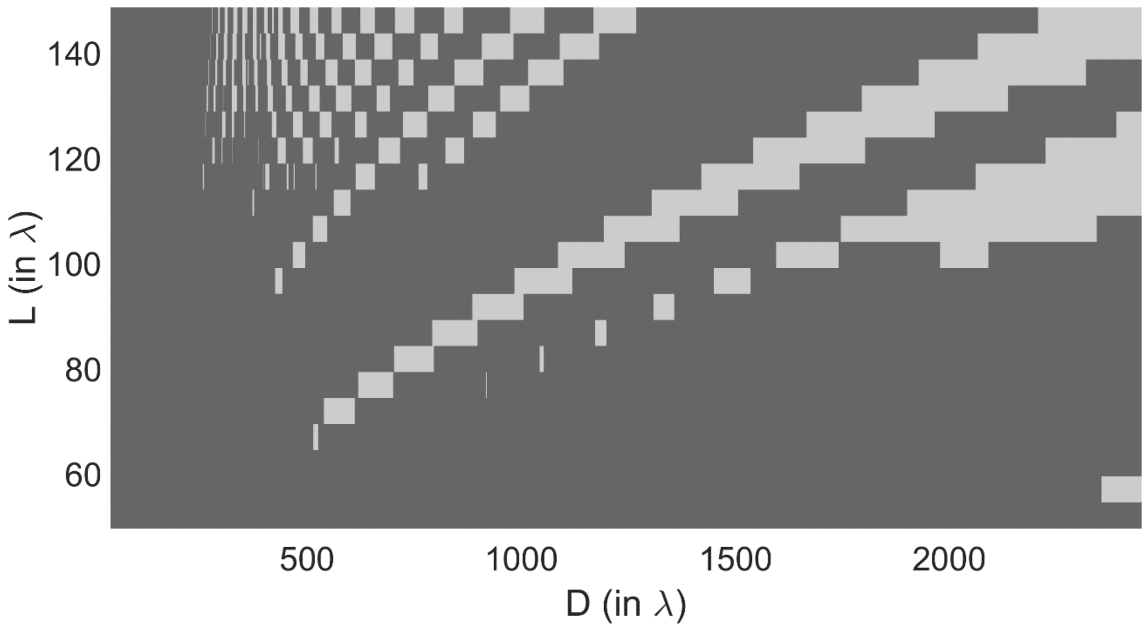

Figure 3. L and D values compliant with all FoM limits in light grey. $R_{mag} \leq 1\ dB$, $\sigma_{mag} \leq 0.25\ dB$, and $R_{phs} \leq 10º$.

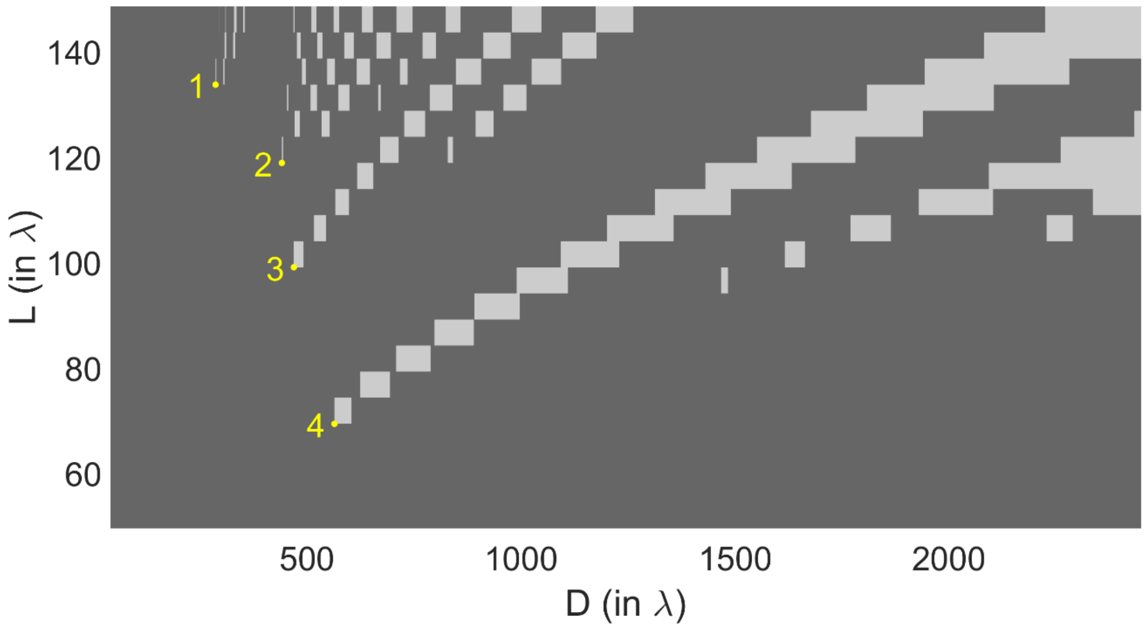

Figure 4. L and D values compliant with all FoM limits in light grey. $R_{mag} \leq 0.9\ dB$, $\sigma_{mag} \leq 0.225\ dB$, *and* $R_{phs} \leq 9º$.

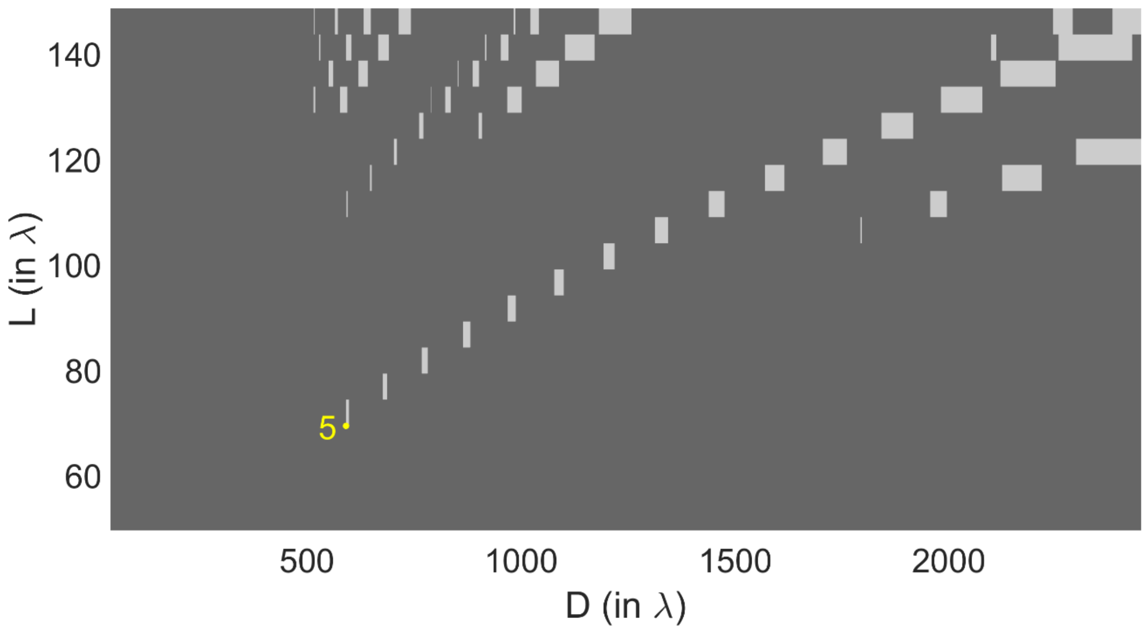

Figure 5. L and D values compliant with all FoM limits in light grey. $R_{mag} \leq 0.8\ dB$, $\sigma_{mag} \leq 0.2\ dB$, *and* $R_{phs} \leq 8º$.

2.4. Effect of chamber array excitation errors

First, an error model was devised, based on the literature, but different from it to keep the complexity down and be able to simulate in an efficient way. It should be noted that, for this study, there were no benefits in in using the literature error models, since they did not really add any depth or interesting effect. This error model consists in a normally distributed complex random variable, that can be expressed as

$$\epsilon_{ch_i} = \mathcal{N}(0, \sigma_{ch}) + j\mathcal{N}(0, \sigma_{ch}), \quad (6)$$

where ϵ_{ch_i} is the excitation error of the i-th AE of the chamber array. Every AE will have an independent realization of this error in each simulation round. σ_{ch} is the standard deviation of the ϵ_{ch_i}. This standard deviation will be varied in a logarithmic scale ($\sigma_{ch_{dB}}$), hence having

$$\sigma_{ch} = 10^{\sigma_{ch_{dB}}/20} - 1. \tag{7}$$

Consequently, the electric field equation (1) will be modified to

$$E_z = \sum_{i=1}^{N_C} (1 + \epsilon_{ch_i}) t_{c_i} \frac{e^{-jkr_i}}{4\pi r_i}. \tag{8}$$

Note that, with this error model, both the complex and real part of the excitation have the same distribution and that the excitation error could make the magnitude of the electric field larger or smaller, also affecting the phase of the excitation.

Having defined the error model, then Monte-Carlo simulations are conducted for the yellow points in Figures 4 and 5, which were selected because they provided the most compact setups in terms of L and D that complied with the stricter FoM tiers. No points were selected from Figure 3 because the most compact L and D combinations did not tolerate almost any excitation error, since they were at the edge of the FoM literature accepted values ($R_{mag} \leq 1\ dB$, $\sigma_{mag} \leq 0.25\ dB$, and $R_{phs} \leq 10º$). In these simulations, the $\sigma_{ch_{dB}}$ started at 0.01 dB and was increased with a 0.01 dB step. Then it was checked if the FoM were fulfilled in the simulated cases and, if they were, then $\sigma_{ch_{dB}}$ was increased another step and so on. The results are shown in Table 1. From them, there is a somewhat clear trend of larger tolerated $\sigma_{ch_{dB}}$ values and larger D. In addition, not all the failures come from the same FoM, and it seems that, for smaller arrays, R_{phs} is more critical and, for larger arrays, R_{mag} is more critical, although that is not very clear and would need to be assessed more carefully. It is also worth mentioning that point 1, which is, by far, the one with the smallest D and, therefore, the most compact setup in terms of chamber dimensions is also the least resilient to the excitation errors. Finally, as expected, point 5, coming from a stricter compliance of FoM, has, by a considerable margin, the upper hand in terms of resilience to excitation errors.

Table 1. Results of Monte-Carlo simulations for the maximum allowed $\sigma_{ch_{dB}}$ while still complying with the FoM literature accepted values. Point numbers correspond to Figures 4 and 5.

Point number	L	IES	D	$\sigma_{ch_{dB}}$ max	Failed FoM
1	1.43 m / 133.65 λ	1.35 λ	3.06 m / 286 λ	0.05 dB	R_{mag}
2	1.27 m / 118.8 λ	1.2 λ	4.73 m / 441 λ	0.12 dB	R_{mag}
3	1.06 m / 99 λ	λ	5.03 m / 469 λ	0.11 dB	R_{mag}
4	0.74 m / 69.3 λ	0.7 λ	6.04 m / 564 λ	0.24 dB	R_{phs}
5	0.74 m / 69.3 λ	0.7 λ	6.33 m / 591 λ	0.5 dB	R_{phs}

2.5. Effect of DUT weighting errors on ZF and MF performance

For this part of the study, the setup is modified by the introduction of two new array antennas. One of them, designed as Interferer Array (IA) and has the same properties as the chamber array, that now receives the name of Main Array (MA), so it has 100 AEs and, as well as for the MA, the IES will be the one corresponding to each of the 5 points of Table 1. Additionally, a DUT array is introduced in the setup, consisting of 49 vertically polarized idealized isotropic sources, with an IES of 0.5λ, which makes it the size of the diameter of the previously considered TZ. The setup can be observed in Figure 6. It can be observed that the DUT array is located within the TZ used before, parallel to the MA, and at the same distance to the centers of both the MA and IA. α_{min} is the minimum angle that can exist between MA and IA without colliding, while being at the same distance D from the DUT array center.

Here, the MA and IA will play the role of two different user equipments and the DUT will play the role of a base station. This can also be seen as an onboard communication unit in a vehicle (DUT) communicating with two access points (MA and IA). The uplink (MA and IA towards the DUT) sum rate is computed to assess the impact on it of DUT weighting errors. Using (1), the channel matrix $\mathbf{H}$ is obtained. This matrix contains all the coefficients from each of the MA and IA AEs to each of the DUT AEs. Then, the weights of the DUT are computed using the well-known ZF ($\mathbf{W}_{ZF}$) and MF ($\mathbf{W}_{MF}$) algorithms, so

$$\mathbf{W}_{ZF} = \mathbf{H}^{\dagger}(\mathbf{H}\mathbf{H}^{\dagger})^{-1}, \tag{9}$$

$$\mathbf{W}_{MF} = \mathbf{H}^{\dagger}. \tag{10}$$

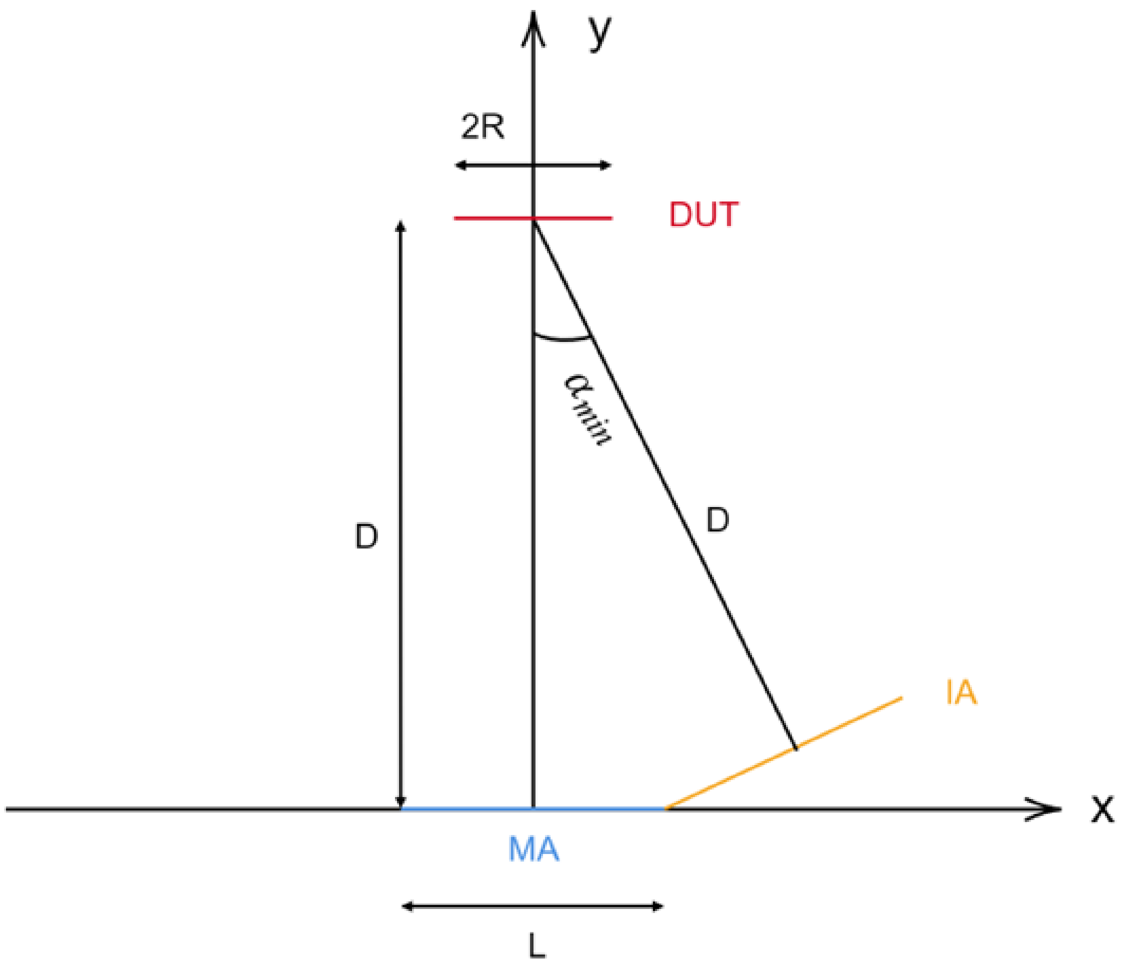

Figure 6. DUT weighting errors study setup

Then, an error is added to those weights ($\mathbf{W}_{ZF}$ and $\mathbf{W}_{MF}$), using the same error model as for the chamber array excitation error done before, with the difference that now the dB scale standard deviation is designed as $\sigma_{DUT_{dB}}$, ranging from 0 to 2 dB, with a 0.1 dB step. On the other hand, different Signal to Noise Ratios (SNRs) are used, in particular, -10, 0, 10 and 20 dB. Afterwards, the Signal to Interference plus Noise Ratios (SINRs) for the MA and the IA are obtained for each $\sigma_{DUT_{dB}}$ and SNR combination. Then, Monte-Carlo simulations were performed, obtaining the average uplink sum rate, computed at each simulation iteration as follows

$$SR = \sum_{u=1}^{2} \log_2(1 + SINR_u), \tag{11}$$

where $SINR_u$ is the SINR of MA ($u = 1$) and IA ($u = 2$). The simulations were carried out for all the 5 points from Table 1, considering two different angles between the MA and IA, namely α_{min} and $\alpha_{min} + 15º$.

Some representative results of the simulations are presented in Figures 7, 8 and 9. In the case of MF, the two extreme cases (points 1 and 5, which have the smallest and largest D and the largest and smallest L, respectively) are presented in Figures 7 and 8, respectively. For ZF, since all the results were qualitatively very similar, only one of the points of Table 1 (point 1) and only for the α_{min} angle has been represented in Figure 9.

From the results, it can be extracted that, as expected, the performance impairment due to the DUT weighting errors is significantly larger for ZF than for MF. It is also worth noting that for ZF, the impact of different angles is almost non-existent, as well as for MF and point 5, whereas for MF and point 1, there are significant differences, but only at SNRs larger than 0 dB. For MF, the rest of the points had a behaviour in between the ones displayed by points 1 and 5.

The DUT excitation error with MF only makes a difference at high SNRs, when the channel is more interference limited than noise limited. Finally, the DUT excitation error with ZF affects higher SNRs more, which makes sense, since the noise has a smaller impact than the interference and if ZF is not correctly applied, then the orthogonality between the MA and IA signals is lost and they interfere each other heavily, leading to a larger decrease of SINR than when the SNR is low. It should also be noted that the decrease of the sum rate is slower the higher the DUT excitation error standard deviation gets, in a somewhat exponential fashion.

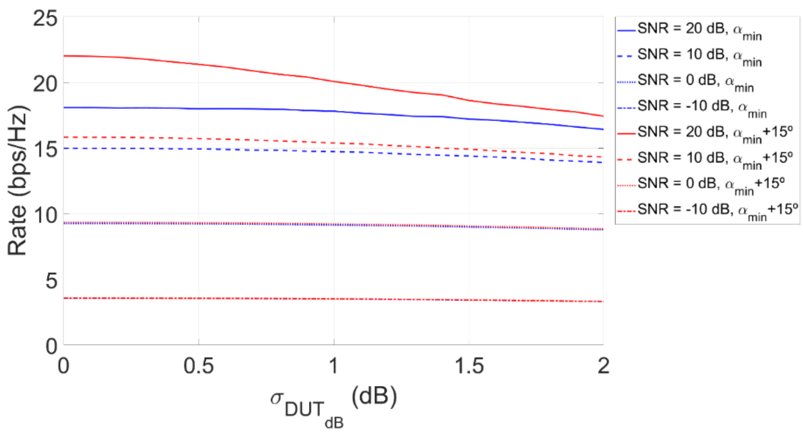

Figure 7. MF average sum rate as a function of $\sigma_{DUT_{dB}}$. L = 133.65λ, D = 286λ (Point 1 of Table 1).

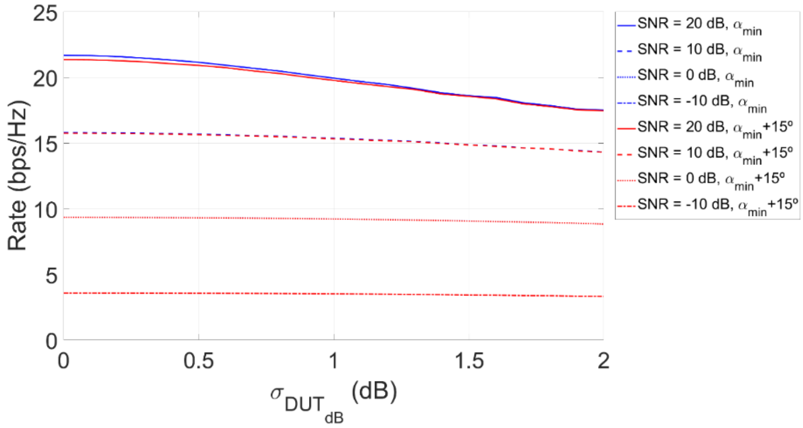

Figure 8. MF average sum rate as a function of $\sigma_{DUT_{dB}}$. L = 69.3λ, D = 591λ (Point 5 of Table 1).

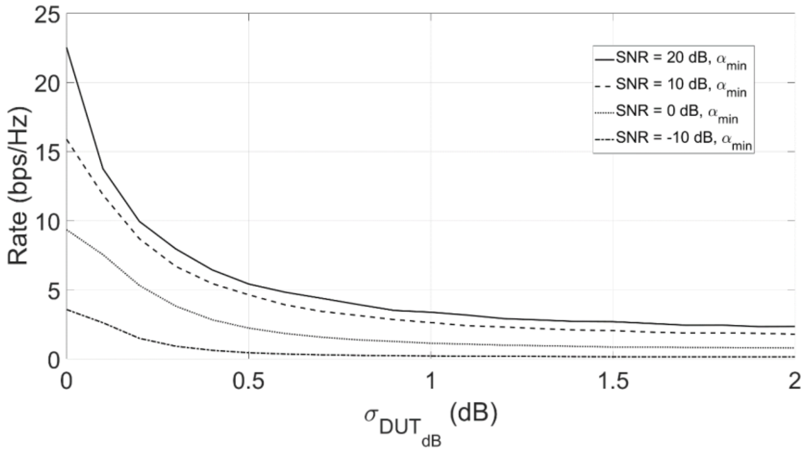

Figure 9. ZF average sum rate as a function of $\sigma_{DUT_{dB}}$. L = 133.65λ, D = 286λ (Point 1 of Table 1).

2.6. Key learnings

From the conducted study, even though it is just a first approach to the design of an OTA testing system at mmWave for vehicular MIMO communications, and has several limitations, there are some key points that can be extracted from it.

As for the results, in short, it can be extracted that OTA setups much more compact than what would be needed from a Fraunhofer distance perspective is possible, however, the consideration of the different sources of error is critical, since they can have a significant effect on the performance of such a system to the point that it could result in a much worse performance, thus making it useless, situation that would suppose relevant costs.

When it comes to the limitations, they include the considered narrowband (just 28 GHz frequency is used), the limited size of the considered test zone, which is 2D only, not considering the AE placement error within the arrays due to manufacturing tolerances, the lack of a proper optimization of the array with several variables, including the number of AEs, the shape of the array (not just ULA), the use of a different tapering, the use of other AEs than isotropic radiators or the consideration of an additional polarization. Some of these limitations can be exploited to obtain better results, whereas some of them will pose a challenge to the simulation times and the feasibility of the system in terms of cost and size, e.g., maybe it is not possible to devise an OTA testing system that can fit a whole vehicle within the test zone, complying with the FoM wit all the possible realistic errors considered, while keeping the cost and dimensions of the chamber low enough for it to be feasible from a business or even research perspective, or maybe it is possible to devise such system, but it requires global optimization so computationally complex that cannot be done in a reasonable time. In any case, this will be explored throughout the duration of the ITN-5VC project.

3. mmWave phased array measurements in reverberation chamber

As part of the secondment at Bluetest, the ESR 2 has conducted a series of measurements using a phased array. One of the measurements is the TRP, which belongs to the active measurements. This report will provide insights into the measurement procedure for such device using the Bluetest reverberation chamber. Additionally, a preliminary analysis of the collected data will be given, focusing on the statistical properties of the data. It is expected to produce a contribution for ISAP 2023 using, at least partially, this data. Additionally, the phased array is from another company (Sivers Semiconductors AB) and some of the specs of the antenna are protected under a Non-Disclosure Agreement, so only basic information will be given.

3.1. Bluetest RTS 65 chamber

A brief description of the key aspects of the Bluetest RTS 65 used for the measurements (serial number 26) related to the phased array TRP measurements at mmWave will be done in this point. Firstly, this reverberation chamber has a size of 1.95x2x1.44 m and is equipped with two moving plates as mode stirrers, along with a turntable of 60 cm of diameter, which can also be used as a mode stirrer. A depiction of a generic RTS 65 chamber can be observed in Figure 10.

Moving to the measurement antennas, aside from sub-6 GHz butterfly antennas, it also has two high frequency antennas, which operate at a frequency between 12 and 43.5 GHz, thus covering all the FR2 frequency bands shown in Figure 1. They are single polarized, but that is not a concern, since polarization balance is reasonably achieved, which has been tested independently both by Bluetest and the ESR2. It can be observed that there is a curved metallic plate between the measurement antennas and the turntable, to obstruct the LOS component. The measurement antennas are connected to the front panel of the chamber, having a 2.92 mm F connector, which is suitable for up to 40 GHz.

The turntable is equipped, among others, with a 1.85 mm F connector (up to 67 GHz), which is connected to another 1.85 mm F connector in the front panel of the chamber, a USB port for communication with the DUT, which is carried over optical fiber inside the chamber to avoid interferences and is routed to a USB-A F at the exterior of the chamber, as well as a F power connector that is routed to another F power connector outside the chamber.

In addition, it has equipped the CATR solution option, but that is not relevant for TRP measurements, since it does not have any effect on such measurements. A roll tower can be installed in the turntable, and the measurements here described have been done using it to hold the phased array. There is the possibility to use the roll tower as a mode stirrer too, but it was not considered necessary, so it was avoided, since it also poses some strain on the power and data cables of the phased array. A depiction of the roll tower can be found in Figure 11, where it can be seen with the Sivers Semiconductors AB EVK02001, which will be detailed later. The reflector of the CATR option can also be observed in that Figure.

Figure 10. Bluetest RTS65 reverberation chamber. Source: https://www.bluetest.se/products/chambers/rts65/

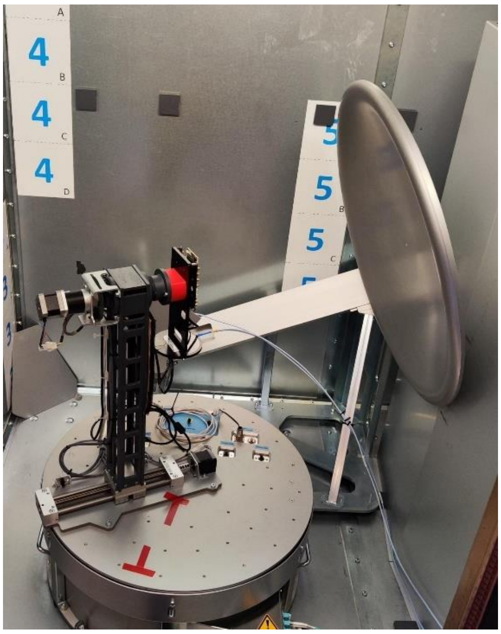

Figure 11. RTS65 26. Roll tower with the Sivers Semiconductors AB EVK02001 mounted.

3.2. Sivers Semiconductors AB EVK02001 and BFM02003 RF module

The EVK02001 is an evaluation kit from the company Sivers Semiconductors AB, which Bluetest had within their DUTs. This evaluation kit includes its own Continuous Wave (CW) source, as well as the software to perform calibration, including a graphical user interface, as well as the possibility of commanding it through a terminal or a script. It comes with a 12 V power supply, and a USB Micro-B cable, needed for the input and output of data. Within RTS65 chamber, the USB cable is connected to the turntable F connector, and from the outside of the chamber to a laptop. As for the power, an external 12 V power supply is used and connected to the power connector outside of the chamber and, from there, to the EVK02001.

The BFM02003 RF module consists of a 2x8 TX phased array (above) and a 2x8 RX phased array (below), which can be used for beam steering of up to $\pm 45º$ in azimuth, with a predefined beambook of 21 beams, with a $4.5º$ step. They will be referred consecutively, in increasing order: Beam 1 ($-45º$), Beam 2 ($-40.5º$), …, Beam 11 ($0º$), …, Beam 21 ($+45º$). This RF module operates at the FR2 frequency bands depicted in Figure 1, covering from 24 GHz up to 29.5 GHz. It is possible to input an I/Q signal and mix it with the CW tone, thus transmitting a wideband signal, although this was not possible due to lack of connections and equipment and could not be implemented in a straightforward way with the existing tools available at Bluetest.

A custom 3D printed holder was manufactured to hold the antenna in the roll tower, courtesy of Bluetest. It can be seen in red in Figure 11.

Figure 12. Sivers Semiconductors AB EVK02001 and BFM02003 RF module. Source: https://www.sivers-semiconductors.com/sivers-wireless/evaluation-kits/evaluation-kit-evk02001/

3.3. TRP measurement procedure

The TRP measurements with the EVK02001 presented here were done at 28 GHz, with the TX module outputting a CW tone, for each one of the different beams. The TRP measurement was selected as a means of evaluating the performance of a phased array, since the TRP can be related to the antenna efficiency, which might not be the same for every single beam, due to effects such as the coupling between elements at different scan angles. Additionally, interesting results can be extracted from this measurement, such as the measured distribution, the required number of samples for a directive antenna at mmWave, the beam correlation or the correlation of one measurement after another, and thus the repeatability. All these results are valuable for both characterizing phased arrays at mmWave as well as designing the measurements and interpreting them.

3.3.1. Chamber loss

The first step in the TRP measurement procedure consists in performing a chamber loss measurement, which will allow to compensate for the losses of the chamber, which will be broken down through this point.

In order to perform a chamber loss measurement, a Vector Network Analyzer (VNA) is required. In this case, a Rohde & Schwarz ZVA67 is used since it is suitable for up to 67 GHz. Additionally, a reference antenna the efficiency of which is known needs to be used. For that purpose, a RF SPIN DRH50 double ridged horn antenna is used, with an operating range of 4.5 to 50 GHz and equipped with a 1.85 mm F connector. In order to have the same chamber load as when the measurement will be performed, the EVK02001 is left over the turntable, while the DRH50 antenna is installed in the roll tower. This can be observed on the left of Figure 13. When doing the chamber loss measurement, the DRH50 will be connected with a 1.85 mm M-M cable to the 1.85 mm F connector of the turntable, which is routed to a 1.85 mm F connector (labelled "Reference antenna") outside of the chamber. One of the ports of the VNA will be connected to that port, both during the calibration and the chamber loss measurements.

Then, before doing the chamber loss measurement, the VNA is calibrated, to leave out of the chamber loss the effect of both 1.85 mm M-M cables of the VNA, as well as the effect of the cables that go from the "Reference antenna" port to the end of the cable that will be connected to the DRH50 antenna. To achieve that, a calibration is performed with the help of an electronic calibration kit, as seen in Figure 12.

Having done the calibration, then the cable of the VNA that is connected to the calibration kit is connected to one of the ports in the front panel of the chamber that is connected to a high frequency measurement antenna. Since the front panel connector is 2.92 mm and the VNA cable is 1.85 mm, a 2.4 mm F (which is compatible with 1.85 mm) to 2.92 M adapter is used. This adapter will be included in the chamber loss measurement.

Therefore, the chamber loss measurement will include, starting from the end of the VNA cable that is the effect of:

- The 2.4 mm F (which is compatible with 1.85 mm) to 2.92 M adapter of the front panel
- The front panel to the high frequency measurement antenna cables and connectors losses
- The high frequency antenna loss
- The pure OTA chamber loss

Note that the loss of the DRH50 antenna is not included in the chamber loss measurement because it is compensated through the software, since the antenna efficiency is known.

The chamber loss measurement will produce a file with, among other data, the S_{21} parameters (complex values).

The most relevant settings for the chamber loss measurement used for the TRP measurements here presented are the following:

- Frequency: 23.5 to 30 GHz, with a 1 MHz step
- Turntable enabled as mode stirrer: for a total of three along with the two plates
- Number of samples: 600, stepped

    - Stepped means that the mode stirrers will move, then stop, the sample sweep will be performed, and they will move to the next of the 600 samples
    - Then when getting the chamber loss as a function of the frequency, the average of the 600 samples at each frequency is performed
- Compensate for the DRH50 antenna

With this chamber loss measurement done, as long as the chamber load is not changed, the same chamber loss will be valid. In the TRP measurements presented here, this was not respected to the strictest level, since the DRH50 antenna as well as the cable that connects it to the turntable were not present when they were done, which supposes a slight change in the chamber load (because the antenna is not made of lossy materials) and, in any case, it would be a fixed bias in the measurement, so unless extreme precision is needed in the absolute value of the measurement, it would not be necessary, since the relative values will have the same statistical properties aside from a small bias in their means. Nevertheless, this effect is probably negligible and well below the uncertainty of the measurement. In addition, the antenna could not be kept inside the chamber all the time since it might be needed to be used by other Bluetest staff. Therefore, for the sake of repeatability and comparability of results, at a very small cost of biasing the collected data, it was decided to not include the DRH50 antenna and cable in the TRP measurement.

Figure 13. Chamber loss measurement setup (calibration)

3.3.2. TRP measurement

Since the EVK02001 has an active TX phased array, and the antenna ports are not designed to be connected to a regular RF cable, then a VNA cannot be used. Therefore, a signal and spectrum analyzer must be used. In this case, a Rohde & Schwarz FSW, which can go up to 67 GHz. The FSW will be connected to the adapter which connects to the port which goes to the high frequency measurement antenna of the chamber (the same to which one of the ends of the ZVA cables were connected).

In this case, since no calibration of the cable is possible with the FSW, the cable loss must be compensated via software. For that, the ZVA is used to perform a cable loss measurement of the cable that will be used to connect the FSW, which is a 1.85 mm M-M. The procedure is as follows:

- Connect both ZVA cables to the calibration kit and perform a calibration
- Connect each ZVA cable to a 1.85 mm F-F adapter
- Connect each end of the cable that will be used with the FSW to the 1.85 F-F adapter's free side
- Perform a cable loss measurement with the same (or larger) frequency range and resolution as the one used for the chamber loss

This is going to introduce a bias to the TRP measurement, since the two 1.85 mm F-F adapter are considered as cable loss, but they are not present during the TRP measurement. This will suppose around 0.4 dB (around 0.2 dB of loss per adapter) of overestimation of the TRP. However, as previously stated, the statistical properties will be the same in terms of distribution, aside from a bias in the mean.

The most relevant settings used for this measurement are the following:

- Use turntable as mode stirrer
- Number of samples: 600, stepped
    - Here the stepped is used for the sake of repeatability, since the positions of the mode stirrers is the same measurement after measurement, provided that the number of samples is kept the same. This means that, e.g., sample number 70 of measurement 1 will have the mode stirrers in the same position as in measurement 2, and thus the field distribution of the chamber will be the same. However, this "same" is limited by the accuracy of the positioners of the mode stirrers, or even the temperature or atmospheric pressure of the chamber (the effect of the latter will probably be less than that of the accuracy of the mode stirrers' positioners) and, in general, the measurement uncertainty.
- Frequency: 27.9997 GHz
    - Frequency span: 0 Hz
    - Resolution and channel bandwidth: 1 MHz
- Compensate for chamber loss
- Compensate for FSW to chamber cable loss
- Use of measurement hook
    - 21 measurements of 15 continuously stirred samples: used as a warmup
    - 21 measurements (1 per each beam) of 600 stepped samples
    - 21 measurements of 600 stepped samples
    - Each of the 21 measurements of 600 stepped samples takes around 24 minutes

The frequency settings are explained by a previous measurement with the FSW, in which it could be seen that the center frequency of the CW tone was not 28 GHz, but closer to 27.9997 GHz. The resolution and channel bandwidth ensured that most (all in practical terms) of the energy outputted by the EVK02001 was captured (the signal power at the peak compared to the level at 0.5 MHz to the left or right of the peak was around 70 dB weaker).

The measurement hook is a tool from Bluetest Flow software, that allows to interact with the measurement via HTTP. Therefore, a Python script was created, with the help of Bluetest staff and using the input from Sivers Semiconductors to configure the antenna, to command the antenna through the measurement, thus not needing to manually interact with the antenna. In each of the 21 measurements of 600 stepped samples, The warmup phase was added after observing that the first measurement used to have a higher TRP than the following ones, and that effect was undesirable, making the results difficult to compare.

Finally, the repetition of the measurement two times (21 times, 600 stepped samples) is performed to check how comparable two measurements with the same mode stirrers' positions are.

The result of the TRP measurement is a file with the value of the measured power (after all the correspondent corrections) at each of the 600 samples, for each measurement (the 15 samples ones are discarded).

3.4. TRP measurement results

Firstly, since a reverberation chamber is designed to obtain a RIMP field distribution, where the power gets exponentially distributed (in linear units, such as mW), it is useful to compare the distribution of the sampled data to that of a pure exponential distribution fitted to the experimental data. An exponential distribution is characterized by a single parameter, λ which equals to the inverse of mean of the distribution, which is also called rate ($1/\lambda$). The probability distribution function is

$$f(x;\lambda) = \begin{cases} \lambda e^{-\lambda x} & x \geq 0, \\ 0 & x < 0, \end{cases} \tag{11}$$

and the Cumulative Distribution Function (CDF)

$$F(x;\lambda) = \begin{cases} 1 - e^{-\lambda x} & x \geq 0, \\ 0 & x < 0. \end{cases} \tag{12}$$

Therefore, to assess if the distribution of the sampled data corresponds to that of an exponential, it can be useful to plot the CDF of the sampled data against that of a fitted exponential distribution. The fitting consists in just using the mean of the sampled data as the rate parameter ($1/\lambda$) of the ideal exponential distribution. Then the fitted distribution is evaluated 10,000 times, to have a smooth CDF.

Since all the plots look very similar, we will just represent one of them. In particular, in Figure 14, the experimental and fitted exponential distribution of beam 10 (-4.5º) of the 21 first measurements is shown. It can be observed that there is a good agreement between the ideal and the empirical distributions. This is similar for all the beams of both measurement sets. It can be observed that the theoretical CDF extends towards further (larger) TRP values, which can be because more samples of the distribution are evaluated, since, for example, when increasing this number to 100,000 times, then the theoretical CDF extends more. However, there is also a consideration about the experimental CDF. This consideration is that the maximum TRP that can be received in an instant is upper bounded by the transmitted power of the DUT itself. Therefore, if you get the least lossy path (due to a combination of constructive interferences and shorter DUT to measurement antenna paths) of all the chamber, then that will be a hard upper bound that will not be able to be trespassed (if we consider that the power output of the DUT is fixed or fluctuates within bounded limits, which is a reasonable assumption).

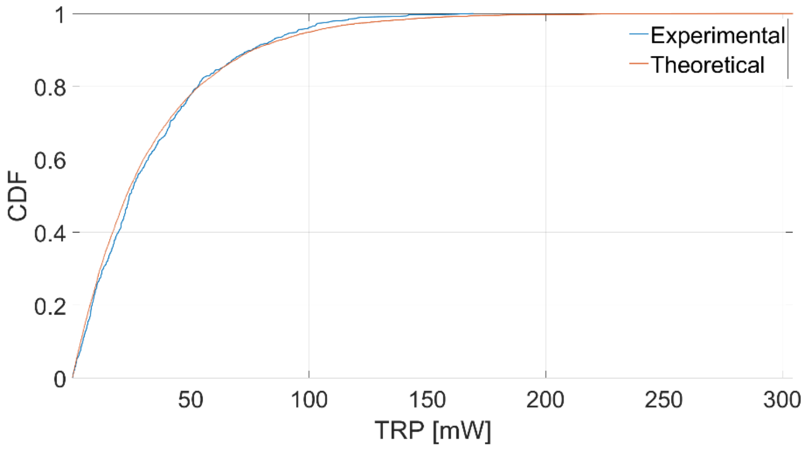

Figure 14. Experimental and fitted exponential distribution of measured RIMP data. Beam 10 (-4.5º), first set of measurements.

On another note, the RIMP environment emulated by the reverberation chamber should be very sensitive to geometrical changes (i.e., mode stirring). One way of checking this is to compute the autocorrelation function of the different measurements, so for each of the 600 samples different measurements (42 in total in this case). Even though it should be studied more carefully, according to the literature [5], a good estimation of the autocorrelation factor can be found if the number of samples is greater than 50 (which happens in this case, since there are 600 samples) and the lag number is below a fourth of the total samples (150 in this case). As an illustrative example, since all the plots look fairly similar, we have the autocorrelation function of the beam 1 (-45°) of the second round of 600 samples measurements in Figure 15, where the autocorrelation coefficient is fairly low for all the considered lags. Therefore, it can be affirmed that, in general, the samples are uncorrelated, as one would expect in a reverberation chamber that emulates a RIMP environment, since each sample corresponds to a different position of the mode stirrers.

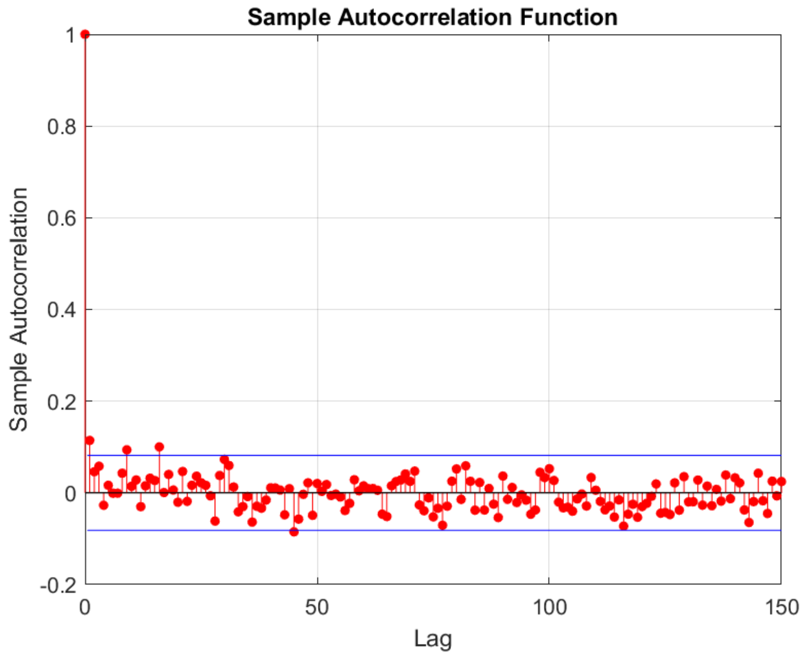

Figure 15. Sample autocorrelation of TRP measurement of beam 1 (-45°) of the second set of measurements.

Another interesting analysis is the correlation of the two consecutive measurement sets. For that, the Pearson correlation coefficient of the time series in linear units (mW) of each beam of the first measurement set is computed with the corresponding beam of the second measurement set. The result is shown in Figure 16. It can be observed that the correlation is, in general, quite high. That means that the results are, in general, fairly repeatable. In fact, for beam 17 ($27º$), the Pearson correlation coefficient is the highest, with an impressive value of 0.9981. However, it is worth noting that the correlation is not that high for the first beams, although it is still rather high, being beam 1 ($-45º$) the one with the smallest Pearson correlation coefficient at 0.92.

A hypothesis that intuitively makes sense is that the antenna temperature, even after the warmup of 21 measurements of 15 samples, which takes around 11 minutes, is not stabilized yet, which, if we assume that a different temperature leads to different results, it will agree with what is seen in Figure 16. This is because the first beam to be measured after the warmup is beam 1 ($-45º$) of the first measurement set, then beam 2 ($-40.5º$) and so on. It is worth noting that every single 600 samples beam measurement takes 24 minutes, so the fact that a clear increase in the correlation is observed for at 5 to 6 beams is noteworthy, since, if the hypothesis is correct, it means that it takes to the antenna to stabilize its temperature between around 2 hours and 11 minutes and 2 hours and 35 minutes.

This hypothesis is partially supported by Figure 17, where the average TRP over the 600 samples is shown for each of the beams and both measurement sets. The largest difference is found at beam 1 ($-45º$), which would agree with the temperature hypothesis (also, if we suppose that a lower temperature gives a higher TRP, it makes sense). However, the difference is no longer relevant for the next beams, or at least not larger than the one experienced by the beams that got very good correlation. Therefore, the temperature hypothesis might not be correct, although it is not clear if it is completely incorrect, since, for beam 1 ($-45º$) it looks like it could be true.

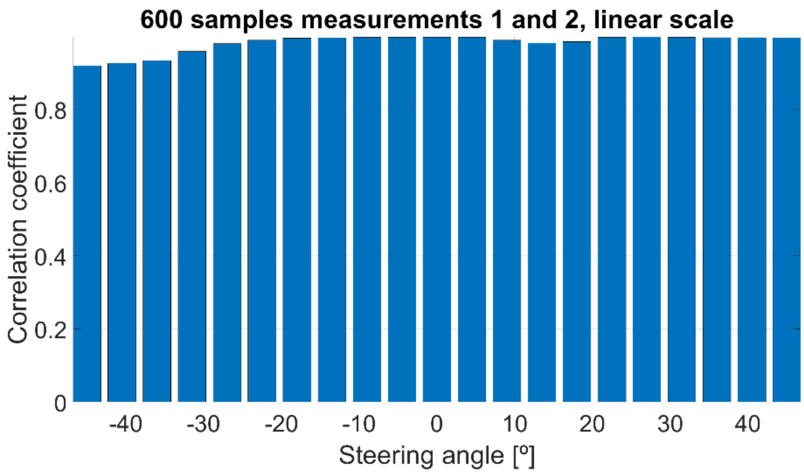

Figure 16. Pearson correlation coefficient of each beam from each measurement set

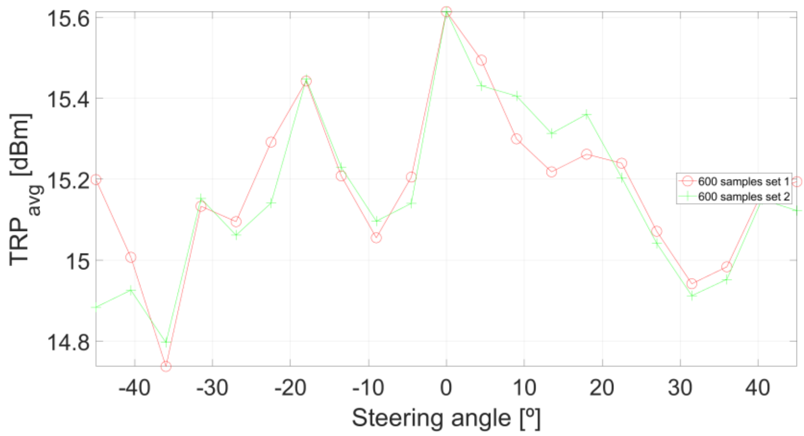

Figure 17. Average TRP for each beam and measurement set

Finally, it is interesting to evaluate how the different beams behave in respect to each other when they are in a practical RIMP environment. For that purpose, the Pearson correlation coefficient is now computed, separately for each of the measurement sets, for each 600 samples time series of each beam and the other beams. To clarify, it means that, the Pearson correlation coefficient will be computed for beam 1 and beam 2, beam 1 and beam 3, beam 1 and beam 4 and so on, belonging all the beams (time series) to the same measurement sets. This is then reflected in Figure 18, which contains the Pearson correlations between the time series of all beams of measurement set 2. Measurement set 1 had similar results. Note that the correlation of the time series of a beam and itself is set to 0, since it would be 1 otherwise and would affect the scale, making Figure 18 more difficult to interpret.

From Figure 18, it is worth noting that there is a significant correlation between adjacent beams. So, for example, the time series of beam 10 ($-4.5º$) and beam 11 ($0º$) have a Pearson correlation coefficient of 0.58. It can also be observed that the correlation diminishes whenever the beams are less adjacent, i.e., the scan angles are further apart. This can be explained by the fact that adjacent beams will share a relevant part of the radiation pattern, causing this that both beams "see" a similar (or at least more similar than further apart beams) field distribution at every position of the mode stirrers. This effect could be considered when evaluating beam selection algorithms, since the possible gain that can be achieved if the best beam is selected at every instant is less when there exists correlation between the beams, because this has the effect of reducing the degrees of freedom of the optimization problem.

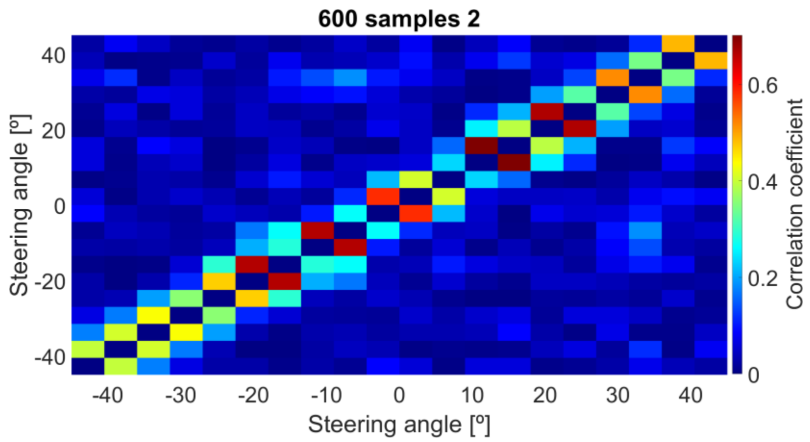

Figure 18. Pearson correlation coefficient among the time series of each beam for measurement set 2

4. Conclusion

This report contributes to the objectives of WP1, since it provides insights about the design process of a compact random-LOS OTA testing system at mmWave, going from the test zone quality characterization and the selection of a set of parameters to meet the required quality while keeping the setup compact, to the relevance of the careful consideration of different sources of error in this design process.

In addition, it describes all the necessary steps to make a TRP measurement at a reverberation chamber, including practical aspects that might not be trivial and that are worth considering, such as adding a warmup phase for an active phased array. Along with this, an analysis of the measured data is performed, checking that the field distribution for a phased array at 28 GHz is in good agreement with theoretical RIMP. The repeatability of the measurements is also explored, achieving good results in terms of linear correlation, and observing a behavior which might be caused due to temperature fluctuations of the phased array. Finally, it is shown that, even in practical RIMP, there is correlation between adjacent beams.

To sum up, this report paves the way towards future OTA characterization of MIMO phased arrays for 5G V2X applications, through a twofold approach, combining the design of an OTA testing solution and the practical characterization of a mmWave phased array in a reverberation chamber.

References

[1] O. M. Bucci, M. D. Migliore, G. Panariello, and D. Pinchera, “Plane-Wave Generators: Design Guidelines, Achievable Performances and Effective Synthesis,” IEEE Transactions on Antennas and Propagation, vol. 61, no. 4, pp. 2005–2018, 2013.

[2] 3GPP. Technical report TR 37.941 V16.2.0, “Radio Frequency (RF) conformance testing background for radiated Base Station (BS) requirements.” 2020.

[3] O. A. Iupikov, P. S. Krasov, A. Alayón Glazunov, R. Maaskant, J. Friden, and M. V. Ivashina, “Hybrid OTA Chamber for Multi-Directional Testing of Wireless Devices: Plane Wave Spectrum Generator Design and Experimental Demonstration,” IEEE Transactions on Antennas and Propagation, pp. 1–1, 2022.

[4] A. A. Glazunov, P.-S. Kildal, and M. S. Kildal, “Devising a horizontal chamber array for automotive ota tests in random line-of-sight,” in 2015 International Symposium on Antennas and Propagation (ISAP), 2015, pp. 1–4.

[5] N. F. Zhang, “Calculation of the uncertainty of the mean of autocorrelated measurements,” Metrologia, vol. 43, no. 4, p. S276, 2006.